Monitoring Intrinsic Optical Signals in Brain Tissue with Organic Photodetectors

Shahab Rezaei-Mazinani, Anton Ivanov, Christopher Proctor, Paschalis Gkoupidenis, Christophe Bernard, George Malliaras, Esma Ismailova

DOI: 10.1002/((please add manuscript number))
Article type: Communication

Monitoring Intrinsic Optical Signals in Brain Tissue with Organic Photodetectors

*Shahab Rezaei-Mazinani, Anton Ivanov, Christopher M. Proctor, Paschalis Gkoupidenis, Christophe Bernard, George G. Malliaras, and Esma Ismailova**

S. Rezaei-Mazinani, Dr. CM. Proctor, Dr. P. Gkoupidenis, Prof. G. G. Malliaras, Dr. E. Ismailova
Department of Bioelectronics, Ecole Nationale Supérieure des Mines, CMP-EMSE, MOC, 13541 Gardanne, France
*Corresponding author email: ismailova@emse.fr

Dr. A. Ivanov, Dr. C. Bernard
Aix Marseille Univ, INSERM, INS, Inst Neurosci Syst, Marseille, France

Keywords: Organic photodetector, bulk heterojunction materials, biomedical devices, intrinsic optical signals, cell volume regulation

Optical measurements are widely used to monitor biological activity and to report changes in metabolism[1], gene expression[2], ionic dynamics[3]. Optical imaging is most commonly implemented combining microscopy with optical sensors like the high affinity silicon photodetectors found in commercially available cameras[3]. In parallel with the development of microscopy and photodetector technology, a variety of methods have been developed to measure biological signals using exogenously applied fluorescent probes that report specific molecules[3] (e.g. for Ca^{2+}, K^{+}), optogenetic strategies that use genetically encoded fluorescent and bioluminescent sensors[4], and measurement of changes in intrinsic optical signals[5,6] (IOS) and metabolic activities[1] (e.g. NADH, FAD). Intrinsic optical imaging is a label-free method that reports metabolic fluctuations that are associated with changes in the intrinsic optical properties of brain tissue.[5,6] It is a valuable tool for measuring physiological and pathophysiological changes in brain function such as epileptiform discharges and disease progression.[7] The measurement of IOSs reflects cell volume changes[8–11], which can be used to track a number of biological events such as propagation of neuronal excitation, hypoxia,

spreading depression[5,6] and blood volume[12]. Therefore, devices measuring IOS can be used as an optical sensing platform for studying various physiological and pathological events. In the brain, ion exchange is the source of electrophysiological activities. Following an action potential, the intracellular ionic concentration changes. The cell volume regulation (CVR) is the mechanism that rebalances the ionic concentration mainly by water flux to reach the physiological conditions. This leads to cell swelling or shrinkage.[5,6,9–11,13] In this way, changes in cell volume result in changes in the scattering or in the transmittance of incident light (i.e. optical properties of the tissue).[5,6] Therefore, IOSs are a measurement of changes in CVR and the detection of these signals as an optical assessment of biological events is important to gain a better understanding of their underlying mechanisms.[10] The most common method for detecting CVR directly or indirectly is measuring IOS using charge-coupled devices (CCD) type of cameras.[14] It has also been shown CVR can be detected using functional magnetic resonance imaging as well.[12] However, these current methods do not provide sufficient temporal resolution for the real-time and simultaneous recording of optical signals and electrophysiological signals. IOS are detected by exposing brain tissue to incident light in the visible spectrum.[5,6] While current methods of optical imaging provide high spatial resolution, a major limitation of IOS is its inability to record signals deep (>200 μm) in the brain due to the limited penetration of visible light in tissue.[3] Implantable and miniaturized photodetectors, light sources and electronics could overcome these limitations by allowing a device that could be placed at any depth.[15] This is not possible with current detector technology found in commercially available devices based on rigid inorganic technology. Implantable inorganic photodetectors embedded in a multi modal probe containing an array of micro-inorganic light emitting diode (μ-ILED) for optogenetic illumination offers promising novel research avenues.[15] However, this work only explored the use of implanted photodetectors for verifying the functioning of μ-ILEDs, rather than for the measurement of weak biological signals. Organic materials and bioelectronic devices[16]

have demonstrated a great deal of interest in plethora of applications, owing to numerous advantages, including thin film architecture, easy and low-cost fabrication, high sensitivity, tunability of physical characteristics, high potential for integration with living tissues and mechanical properties ideal for in vivo applications.[17–23] Organic optoelectronic devices have recently been used in biomedical applications. An organic photovoltaic device was used for neuronal photoactivation[24] and to provide visual cues to blind retina[25], it showed the potential of organic electronics to restore light sensitivity in blind retinas [26] and also showed the promise as a fully organic retinal prosthesis for restoring vision in case of degenerative blindness[27]. Polymer optoelectronic devices have also been used for interfacing with the retina to restore light sensitivity and to stimulate the blind retina[28]. In both of these examples, the generated photocurrent has been utilized for stimulation. Organic photodetectors (OPD) have also been explored as ultraflexible skin-based sensors. In this case, the integration of organic light emitting diodes and OPD on a flexible substrate was used to measure blood oxygen levels cutaneously.[29] To the best of our knowledge, OPDs have not been utilized as optical sensor in the brain for detecting biological signals. In the present work, we aim to broaden the biomedical application of organic photodetectors by demonstrating their utility and high temporal resolution for recording of changes in brain tissue's optical properties caused by CVR during both pathophysiological conditions and physiological conditions. In order to measure real time changes in intrinsic optical signals in live brain tissue, a customized setup was designed featuring a brain tissue slice in a perfusion bath with electrodes for recording electrophysiology activity as well as an electrical stimulation electrode (**figure 1a**). During both experiments, the neuronal network activity was recorded as a change in local field potential (LFP) in CA1 region (**figure 1b**) using an extracellular electrode. The setup featured a halogen based illumination source, which was placed underneath the perfusion bath for illuminating the brain slice. In order to record IOS from the specific region of the tissue (14 mm^2), a microscope was utilized in order to collect the

transmitted light to focus it on the OPD mounted at the top of the setup (figure 1a). The OPD was used to measure changes in the transmittance of light through the brain slice caused by cell volume changes due to ion fluxes in and out of the cells making up the brain tissue. The photodetector was designed to have minimal layers and low leakage current in order to simplify the fabrication process and maximize sensitivity (**figure 1c**). The structure consisted of a thin semi-transparent gold (Au) electrode on a glass substrate, Poly(3-hexylthiophene-2,5-diyl) (P3HT) blended with [6,6]-Phenyl C60 butyric acid methyl ester (PCBM) as the photoactive layer and an aluminum (Al) as the cathode (figure 1c). Finally, the device was encapsulated using epoxy and a glass cover-slip. The device presented a low dark-current and a linear response to incident light intensity as is typical of high performing OPDs (**figure 1d**).[30]

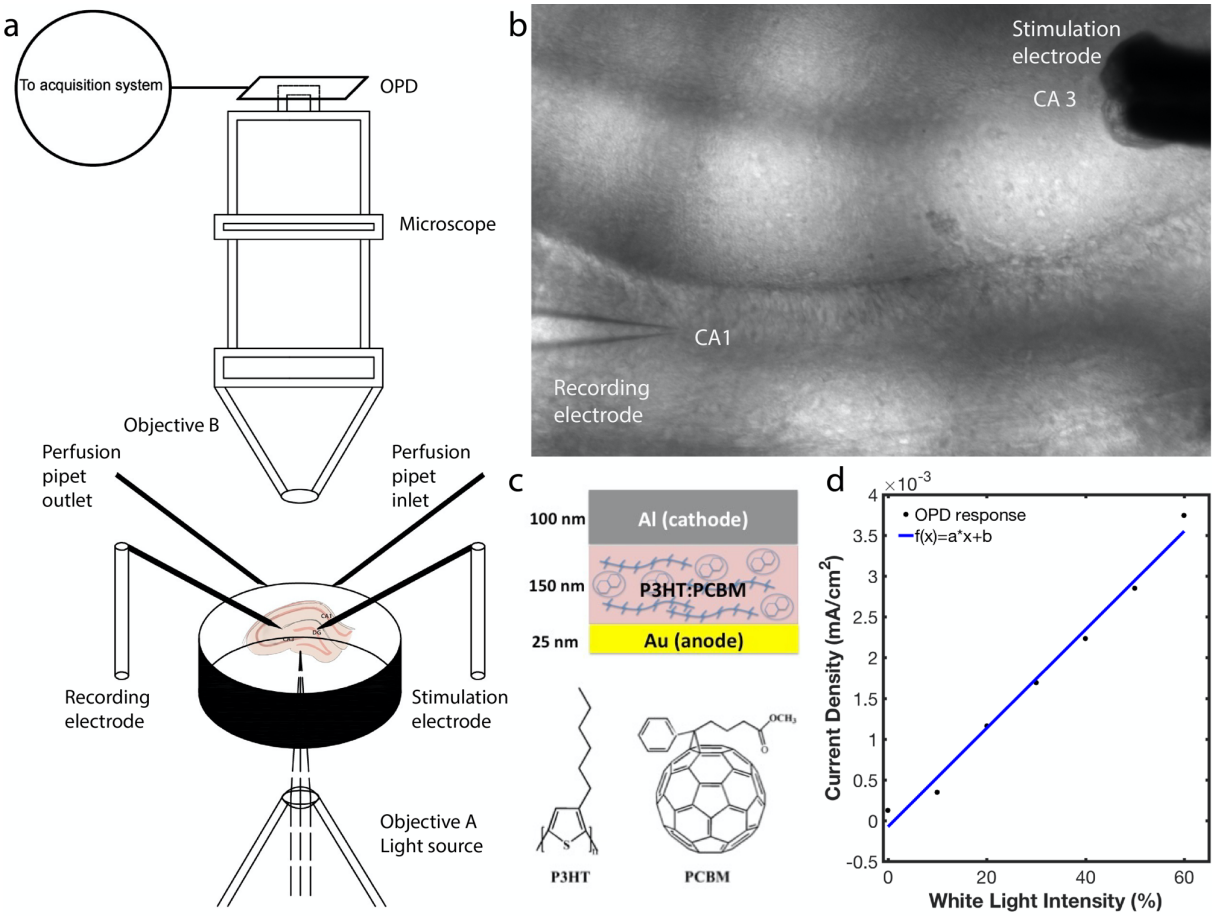

Figure 1. **Characteristics of the OPD and the experimental setup. a)** Lens A focuses the light onto the region of interest and lens B collects the transmitted light from the tissue. The OPD was installed on top the microscope to detect optical changes and to avoid any optical

perturbations caused by the perfusion solution flow. **b)** The area of interest was at the surface of the hippocampal slice, where the overall optical activity of the neuronal network was recorded. The stimulation electrode was implanted in the CA3 region to evoke synaptic response and the recording electrode was located in the CA1 region. **c)** OPD structure including a semi-transparent Au-anode, a P3HT:PCBM blend film and Al as the cathode. **d)** Linear response of current density to the stepwise increase of illumination intensity shows the good performance of the OPD. The OPD was biased at -0.3V to maximize the photogenerated carrier.

In the first experiment, we recorded IOS during epileptiform discharge, induced by 4-aminopyridine (4AP), a non-specific inhibitor of voltage-gated potassium channels. This drug is widely used in the field of experimental epileptology, since it evokes long-lasting (> 3 hrs) and spontaneous epileptiform activity.[31,32] The OPD's generated current was recorded simultaneously with electrophysiological activities (extracellular field potentials). Induction of the epileptiform activity took about 15 minutes (**figure 2a**) after the application of 4-AP and lasted over the entire period of the drug application (about 25 minutes). A synchronous excitation occurred spontaneously involving not only CA1 pyramidal cells but all the neurons of the slice's network. The initial phase consisted of a set of collective and regular LFPs, indicating the overall excitation of the network. The first phase, showing the highly intense epileptiform activity (figure 2a) lasted approximately 1 min (time interval: 15-16), then the intensity and the amplitude of the activity gradually decreased. This second phase, the decreasing period (time interval: 16 to the end), consisted of group epileptiform discharges occurring every 0.5 to 2 seconds. The OPD's generated current started to rise 12 seconds after the epileptiform discharge onset and reached its maximum (7.5%) almost 2 minutes after the peak of the epileptiform activity (**figures 2b**). IOS's temporal delay is probably due to the fact that the transmembrane water flow (CVR's effect), responsible for the cell swelling, is a slower process than the ion flux required for the generation of LFP changes. When the amplitude of the epileptiform activity decreased (**figure 2c**), the transmittance of slice decreased as well (**figure 2d**). Spectro-temporal analysis of the electrophysiological signal (**figure 2e**) showed that the decrease of epileptiform activity's spectral power was followed

by a decrease in transmittance (figure 2d). Here, it was demonstrated that the epileptiform discharge caused significant changes in translucency of the tissue due to cell swelling. This effect was detected by the OPD. These results demonstrate that the OPD is a promising device for studying strong signals (more than 5% optical changes) typical of pathophysiological events, e.g. epileptiform discharges.

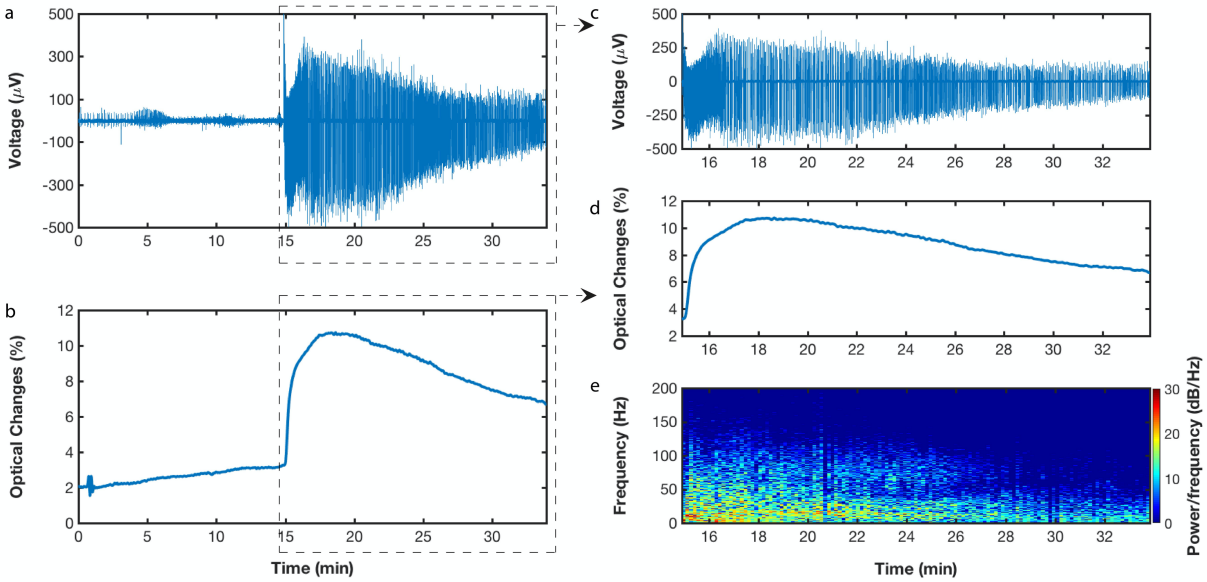

Figure 2. OPD detects optical changes with the same temporal resolution as simultaneously recordings electrophysiological signals during pathological epileptiform activity. Inhibition of voltage-gated potassium channels by bath application of 4-AP induced paroxysmal electrophysiological activity in hippocampal slices of an adult mouse. Paroxysmal activity is associated with a dynamic change in the tissue optical properties. **a)** 4-AP induced activity is characterized by rapid oscillations of extracellular LFP. **b)** OPD generated current expressed as a percentage of the baseline value. OPD exposed to the white light transmitted through the tissue slice generates a current proportional to the light intensity. Variations in slice's optical properties modulate the transmitted light intensity that induces a variation of the electrical current generated by OPD. Note that cell swelling is already detectable as soon as 4-AP is washed in (between t=0 and t=15 min), whilst field oscillations are barely visible. At the beginning of 4-AP wash in, cells start to fire, but not in coordinated fashion. The latter occurs abruptly around t=15 min. **c)** Zoom in of the paroxysmal activity of **a**. **d)** Zoom in on the variations of optical properties of the slice of **b**. Temporal comparison of the figures c and d shows the delayed beginning of the augmentation of transmittance with respect to electrophysiological activity, which is due to the slow dynamics of cell swelling. **e)** Spectro-temporal representation of the LFP change illustrated on **d.** OPD generated current decreases simultaneously with a decay of electrophysiological activity power evaluated by spectro-temporal analysis of the LFP.

In the second experiment, we wanted to determine if the sensitivity of the OPD was high enough to detect lower-level IOSs (below 5% optical changes) generated by physiological events at tissue and even cellular levels (e.g. neuronal network activity). In this experiment, IOS was induced with physiological synaptic activation, which is much smaller than epileptiform activity. For this reason, a bipolar metal stimulation electrode was implanted in *Stratum Radiatum* close to the CA3 region (figure 1b). The electrical stimulation of Schaffer collaterals induced synchronous excitation of hundreds of CA1 pyramidal cells. This network activity was evoked using two trains of electrical pulses generated with 10 Hz frequency (**figure 3a**). The response to synaptic stimulation was characterized by lower amplitude IOS. The duration of the first stimulation cycle was 30 seconds and the second cycle duration was 10 seconds. The maximum optical changes induced by both stimulation trains were approximately 3%, and the activities were significantly distinguishable from the noise level, 0.3% (root mean square of noise level expressed in percentage). In combination with the previous results, this signifies that the OPD can detect a high range of optical signals associated with neuronal activities of different ranges of intensity. When the network activity was induced, the transmittance started to increase to the maximum point (**figure 3b**), which denotes that the CVR increases due to cell swelling. Both the trend and the magnitude of changes in IOS further confirm the OPD's performance and also validate its versatility for detecting both low and strong signals. The spontaneous activity that was detected in the slice before electrical stimulation, persisted also after it. This suggests that the synaptic activation did not induce any depolarization block, and therefore, the evoked neuronal network activation remained in physiological range. In order to analyze the electrophysiological signal in the spectro-temporal domain, high-amplitude-bipolar stimulation artifacts were suppressed (**figure 3c**) using a custom-made program. From the beginning of the first synaptic activation until the second, a comparison between the optical signal (**figure 3d**) and spectro-temporal analysis of the same interval (**figure 3e**) was conducted. During synaptic stimulation (interval

A) the LFP's spectral power was high but decaying while IOS amplitude was low and slowly rising. The high spectral power of electrophysiological activities during stimulation in this interval led to blockade of the neuronal network and consequently, potentially blocked CVR's activity for a period of time, therefore cell swelling was not very pronounced. This phenomenon can be seen as slow changes of the IOS during a part of the synaptic activation period (interval A). After evoking the network activity (interval B), the LFP power decreased (figure 3e), whereas IOS continued to rise. Afterwards, when the electrophysiological activity returned to its initial level (interval C), the IOS started to decay (figure 3d). Thus, in the case of short lasting (seconds) physiological neuronal network activity, the IOS did not follow the LFP as it did in case of long lasting (minutes) epileptiform discharges. However, in both cases the OPD showed high sensitivity to detect the neuronal activation induced changes in the optical properties of the neuronal tissue. In order to examine the responsiveness of our OPD to physiological changes weaker than the first synaptic activation, an electrical stimulation of 10 seconds (figure 3a) was applied before IOS reached the baseline (figure 3b). It was observed that when stimulation was applied, the trend of the IOS that was decreasing halted, and immediately after the second synaptic activation, IOS increased towards the maximum level. Subsequently, the IOS decreased gradually until reaching the baseline. Thus, the OPD presented a high sensitivity and temporal resolution in such short-duration physiological events. This demonstrates that monitoring of optical properties using OPD could be a novel complementary approach to electrophysiology for detecting changes in brain tissue that may otherwise go unnoticed. To the best of our knowledge this is the first report of simultaneous, temporally-resolved recording of electrophysiological and IOS using OPD. These results indicate that OPD used in conjunction with electrophysiological recordings can provide a platform for studying how certain biological events and IOS are correlated thereby leading to a better understanding of their mechanism.

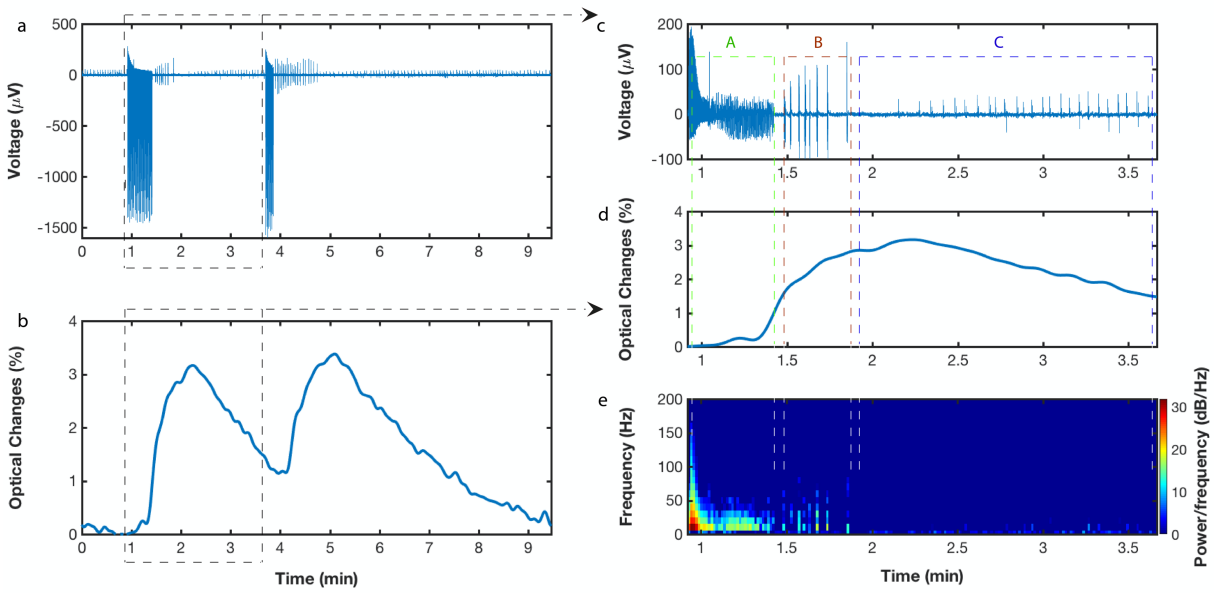

Figure 3. OPD can detect weak physiologically-relevant IOS evoked by neuronal activities. Neuronal network activity induced by electrical stimulation is modulating the transmitted light, whose intensity changes were detected by the OPD **a)** LFP responses to 10-Hz electrical stimulation for 30 and 10 sec recorded in hippocampal slice of adult mouse brain. Spontaneous activity detected in slice before electrical stimulation persisted also after it. This suggests that the stimulation did not induce a depolarization block and that induced neuronal network activation remained in physiological range. **b)** Responses to both stimulation events were accompanied by changes in the electrical current generated by the OPD. **c)** Zoom in on the first response to synaptic activation, where the stimulation artifacts are suppressed. **d)** Zoom in on the tissue's optical response to the first electrical stimulation. During the stimulation (interval A) the optical changes were slow but became faster in the end of stimulation train. Optical signal continued to rise during after-discharge (interval B) and started to decay slowly when network activity returned to its initial, before stimulation level (interval C). **e)** Time-frequency-power presentation of the LFP signals during and after the first cycle of synaptic activation. During synaptic stimulation the LFP power was high and then decayed whereas IOS amplitude was low but slowly rising. After stimulation the LFP power decreased whereas IOS continued to rise and started to decay when the electrophysiological activity returned to its initial level (**figure 2d**). Thus, in the case of short lasting (seconds) physiological neuronal network activity the IOS did not follow the LFP as it did in case of long lasting (minutes) paroxysmal discharges. However in both cases the OPD showed sensitivity sufficient to detect the neuronal activation induced changes in optical properties of the neuronal tissue.

In conclusion, we presented an IOS recording platform using simple OPDs. We demonstrated the capability and potential impacts of this system for the detection of intrinsic optical signals, an important phenomenon caused by changes in cell volume. The OPDs were shown to have high sensitivity and high temporal resolution, allowing for detection of a wide range of pathophysiological and physiological events. Though we focused on IOS here, the tunable

properties of OPD will allow this platform to be adapted for other optical based sensing applications in living tissues including monitoring metabolic activities. Detection of such events in specific regions of the brain and in a population of cells or even individual cells, will improve understanding of metabolic and physiological activities. Further improving its utility, we anticipate that this OPD based platform can be miniaturized to make implantable devices allowing for in vivo sensing. We anticipate that the simplicity of this OPD based platform combined with its exceptional sensitivity and temporal resolution will prove an invaluable tool for numerous biological applications.

Experimental Section

***Organic Photodiode Fabrication and Characterization*:** Devices were fabricated using standard microfabrication procedure. Microscope glass-slides of 25mm75mm as substrate were cleaned. Transparent anode of 40 nm thicknesses was defined using sequential thermal evaporation of 10 nm Cr and 30 nm Au on pre-patterned S1813 photoresist and a subsequent soaking in an acetone-isopropanol bath for removing the excess material. The Cr layer was used underneath of Au for the enhancement of the surface adhesion of Au to glass. Active layer was spun at 1000 RPM for 2 minutes to achieve 150 nm thicknesses (determined using optical profilometer Veeco) solution blend of P3HT and PCBM at a weight ratio of 1:1 in 1,2-dichlorobenzene at an overall concentration of 40 mg/ml. Solution was heated and stirred overnight at 90^{o}C prior to casting. Film was heated for 15 min at 110^{o}C under inert atmosphere to drive off residual solvent and to stabilize. Cathode was deposited using thermal evaporation of 100 nm of Al and covered with shadow mask. The achieved active area was 14 mm^2. For device encapsulation, epoxy (Ossila-E131) in conjunction with glass coverslip was UV-cured at the wavelength of 365nm for 2 min under inert atmosphere. Device characteristics were measured under dark conditions using Keithley 2612A source-meter.

Tissue Slice Preparation: A mouse anaesthetized with isoflurane was decapitated; the brain was rapidly removed from the skull and placed in the ice-cold artificial cerebrospinal fluid (ACSF). The ACSF solution consisted of (in mmol/L): NaCl 126, KCl 3.50, NaH2PO4 1.25, NaHCO3 25, CaCl2 2.00, MgCl2 1.30, and dextrose 5, pH 7.4. ACSF was aerated with 95% O2/5% CO2 gas mixture. Saggital slices (350 μm) were cut using a tissue slicer (Leica VT 1200s, Leica Microsystem, Germany). During cutting, slices were submerged in an ice-cold (< 6°C) solution consisting of (in mmol/L): K-gluconate 140, HEPES 10, Na-gluconate 15, EGTA 0.2, NaCl 4, pH adjusted to 7.2 with KOH. Slices were immediately transferred to a multi-section, dual-side perfusion holding chamber with constantly circulating ACSF and allowed to recover for 2h at room temperature (22°C-24°C).

Synaptic Stimulation and Field Potential Recording: Ex-vivo LFP and patch-clamp recordings were performed on brain slices from P21-56 OF1 male mice. Slices were transferred to a recording chamber continuously superfused (15ml/min) with ACSF (33–34°C) with access to both slice sides. Schaffer collateral/commissures was stimulated using the DS2A isolated stimulator (Digitimer Ltd, UK) with a bipolar metal electrode. Stimulus current was adjusted using single pulses (40-170 μA, 200μs, 0.15 Hz) to induce LFP of about 50% maximal amplitude. LFPs were recorded using glass microelectrodes filled with ASCF, placed in stratum pyramidale of CA1 area and connected to the ISO DAM-8A amplifier (WPI, FL). Synaptic stimulation consisting of a stimulus train (200μs pulses) at 10 Hz lasting 30s was used to induce slice tissue optical response. To induce epileptiform activity a Kv1 channel blocker 4-aminopyridine (4AP, 50 μM) was added to ACSF.

Experimental setup: The illumination intensity was kept at 50% of the maximal power during the induction of both epileptiform and physiological activity. At this power the halogen lamp used for the illumination produced light of stable intensity

Data Analysis: Data analysis and signal processing were done using Matlab R2016b.

Acknowledgements

The authors acknowledge Alexandra Rutz, Ph.D. and Professor Rodney O'Connor from the department of Bioelectronics for fruitful discussions and valuable inputs. The fabrication of the device was performed at the Centre Microelectronique de Provence (CMP). The authors thank Gaelle Rondeau and the staff of the clean room in CMP for technical support during the device fabrication.

Received: ((will be filled in by the editorial staff))
Revised: ((will be filled in by the editorial staff))
Published online: ((will be filled in by the editorial staff))

References

[1] K. A. Foster, F. Galeffi, F. J. Gerich, D. A. Turner, M. Müller, *Progress in Neurobiology* **2006**, 79, 136.

[2] Y. Shav-Tal, R. H. Singer, X. Darzacq, Nature Reviews *Molecular Cell Biology* **2004**, 5, 855.

[3] C. Grienberger, A. Konnerth, *Neuron* **2012**, 73, 862.

[4] K. Deisseroth, *Nature Neuroscience* **2015**, 18, 1213.

[5] P. G. Aitken, D. Fayuk, G. G. Somjen, D. A. Turner, *Methods* **1999**, 18, 91.

[6] D. Fayuk, P. G. Aitken, G. G. Somjen, Turner, *Journal of Neurophysiology* **2002**, 87, 1924.

[7] M. Haglund, G. Ojemann, D. Hochman, *Nature* **1992**, 358, 668.

[8] F. Lang, *Nestle Nutrition Institute workshop series* **2011**, 69, 115.

[9] B. Friedrich, I. Matskevich, F. Lang, *Contributions to nephrology* **2006**, 152, 1.

[10] T. Cesetti, F. Ciccolini, Y. Li, *Frontiers in Cellular Neuroscience* **2012**, 6, 3.

[11] T. J. Jentsch, Nature Reviews *Molecular Cell Biology* **2016**, 17, 293.

[12] Y. Ma, M. A. Shaik, M. G. Kozberg, S. H. Kim, J. P. Portes, D. Timerman, E. M. C. Hillman, *Proceedings of the National Academy of Sciences* **2016**, 113, E8463.

[13] K. Holthoff, O. Witte, *J. Neurosci.* **1996**, 16, 2740.

[14] R. Andrew, B. Macvicar, *Neuroscience* **1994**, 62, 371.

[15] T. Kim, J. G. McCall, Y. Jung, X. Huang, E. R. Siuda, Y. Li, J. Song, Y. Song, H. Pao, R. Kim, C. Lu, S. Lee, I. Song, G. Shin, R. Al-Hasani, S. Kim, M. Tan, Y. Huang, F. G. Omenetto, J. A. Rogers, M. R. Bruchas, *Science* **2013**, 340, 211.

[16] M. Berggren, A. Richter-Dahlfors, *Advanced Materials* **2007**, 19, 3201.

[17] T. Someya, Z. Bao, G. G. Malliaras, *Nature* **2016**, 540, 379.

[18] D. Khodagholy, J. Gelinas, Z. Zhao, M. Yeh, M. Long, J. Greenlee, W. Doyle, O. Devinsky, G. BuzsÃki, *Sci. Adv.* **2016**, 2, e1601027.

[19] D. Khodagholy, J. N. Gelinas, T. Thesen, W. Doyle, O. Devinsky, G. G. Malliaras, G. Buzsáki, *Nature Neuroscience* **2015**, 18, 310.

[20] D. Khodagholy, T. Doublet, P. Quilichini, M. Gurfinkel, P. Leleux, A. Ghestem, E. Ismailova, T. Hervé, S. Sanaur, C. Bernard, G. G. Malliaras, *Nature Communications* **2013**, 4,

1575.

[21] D. Khodagholy, T. Doublet, M. Gurfinkel, P. Quilichini, E. Ismailova, P. Leleux, T. Herve, S. Sanaur, C. Bernard, G. G. Malliaras, *Advanced Materials* **2011**, 23, H268.

[22] Williamson, Rivnay, Kergoat, Jonsson, Inal, Uguz, Ferro, Ivanov, Sjöström, Simon, Berggren, Malliaras, Bernard, *Advanced Materials* **2015**, 27, 3138.

[23] J. Rivnay, R. Owens, G. G. Malliaras, *Chemistry of Materials* **2014**, 26, 679.

[24] D. Ghezzi, M. R. Antognazza, M. D. Maschio, E. Lanzarini, F. Benfenati, G. Lanzani, *Nature Communications* **2011**, 2, 166.

[25] Gautam, Rand, Hanein, Narayan, *Advanced Materials* **2014**, 26, 1751.

[26] D. Ghezzi, M. R. Antognazza, R. Maccarone, S. Bellani, E. Lanzarini, N. Martino, M. Mete, G. Pertile, S. Bisti, G. Lanzani, F. Benfenati, *Nature Photonics* **2013**, 7, 400.

[27] J. F. Maya-Vetencourt, D. Ghezzi, M. R. Antognazza, E. Colombo, M. Mete, P. Feyen, A. Desii, A. Buschiazzo, M. Paolo, D. Marco, F. Ticconi, L. Emionite, D. Shmal, C. Marini, I. Donelli, G. Freddi, R. Maccarone, S. Bisti, G. Sambuceti, G. Pertile, G. Lanzani, F. Benfenati, *Nature Materials* **2017**, DOI 10.1038/nmat4874.

[28] N. Martino, P. Feyen, M. Porro, C. Bossio, E. Zucchetti, D. Ghezzi, F. Benfenati, G. Lanzani, M. R. Antognazza, *Scientific Reports* **2015**, 5, 8911.

[29] T. Yokota, P. Zalar, M. Kaltenbrunner, H Jinno, N. Matsuhisa, H. Kitanosako, Y. Tachibana, W. Yukita, M. Koizumi, T. Someya, *Science Advances* **2016**, 2, e1501856.

[30] C. M. Proctor, M. Kuik, T. Nguyen, *Progress in Polymer Science* **2013**, 38, 1941.

[31] R. D. Traub, S. B. Colling, J. G. Jefferys, *The Journal of physiology* **1995**, 489 (Pt 1), 127.

[32] H. J. Luhmann, V. I. Dzhala, Y. Ben-Ari, *The European journal of neuroscience* **2000**, 12, 2757.